SAFETY BRIEF

On the Safety of a Portable Grinder Guard[*]

by Dennis B. Brickman[**] and Ralph L. Barnett[***]

ABSTRACT

A rigid body mode of failure has been identified in two piece adjustable grinding wheel guards for portable grinders. Under the action of a fragment storm, the upper portion of the guard may tilt and allow an escape displacement to develop at the leading edge of the protective skirt. Three approaches are described for analyzing this behavior: a very rough analytical investigation, static testing, and dynamic wheel breakage testing of the guard. Each reveals the shortcomings of the commercially available guard.

INTRODUCTION

The American National Standards Institute has developed a standard entitled American National Standard Safety Code for Portable Air Tools, ANSI B186.1-1975 (1). For types 27 and 28 depressed center grinding wheels, paragraph 3.2.9.4(3) states the following requirements:

"A safety guard for vertical or angle grinders using Types 27 and 28 wheels shall cover the wheel's plane of rotation toward the operator for at least 180 degrees, shall cover the side of the wheel toward the driving flange for at least 180 degrees, and shall have a lip on the outer edge which curls inward to deflect wheel fragments and to provide necessary strength. The lip shall extend outside the face of the wheel throughout the 180 degree coverage" (2).

ANSI's illustration of a typical guard for a type 27 wheel is reproduced in Fig. 1 (3). It should be noted that this guard is a one piece nonadjustable guard. Guards of this type have been dedicated to the type 27 or 28 wheel. Some manufacturers use a single guard of this type for both type 27 and type 28 wheels that are 17.8 cm (7 in.) in diameter. This single guard approach is functionally incompatible with both type 27 and type 28 wheels that are 22.9 cm (9 in.) in diameter because of the greater disparity in wheel height.

A type of depressed center wheel guard which is not characterized by ANSI can be described as a two piece adjustable guard that is functionally compatible with both type 27 and 28 wheels. This guard is illustrated in Fig. 2 in the fully retracted position which is compatible with the type 27 wheel. The vertical adjustment and basic construction of this guard are similar to the wheel guards described by ANSI for vertical grinders used with type 6 and type 11 cup wheels. Although the requirements are almost identical for the depressed center and cup wheel guards, in practice the cup wheel guards encircle 270 degrees compared to the 180 degrees used for depressed center wheel guards. Industry testing of single piece depressed center wheel guards and of 270 degree cup wheel guards has provided the protection anticipated by ANSI in the guarded sectors. With this experience base coupled with the observation that the thickness used in the adjustable depressed center wheel guard is over 25% greater than its single piece counterpart, intuition would suggest that the structural integrity of the adjustable depressed center wheel guard will be sufficient to provide the protection required by ANSI. Unfortunately, intuition is a good servant, but a bad master. When adjusting two piece guards, care must be exercised to maintain parallelism between the upper and lower guard portions so that an escape geometry does not develop in the guarded segment which would allow broken wheel fragments to escape. The fragments themselves may force the upper guard into a nonparallel orientation relative to the wheel's plane of rotation, thus achieving the escape geometry which destroys the guarding capability.

The bolted joints connecting the upper guard to the lower guard utilize vertical slots which allow both rotation and sliding at the location of bolts 1 through 4. At all positions, from the fully retracted to the fully extended, the upper guard can achieve a rotation of approximately 11°. When the grinding wheel is in a horizontal position, the upper guard can be rotated in a plane which is perpendicular to the line between bolts 1 and 4. This rotation α illustrated in Fig. 3 for the fully extended and the fully retracted initial positions always produces the same total sliding of the bolts at locations 1 through 4. Furthermore, the joints at bolts 1 and 4 always undergo a rotation of α and the joints at bolt locations 2 and 3 rotate through an angle whose component in the plane of rotation is α. The rigid body rotation α gives rise to a displacement Δ of the leading edge of the upper guard.

The upper surface of the grinding wheel is typically set anywhere from zero to 6.35 mm (0.25 in.) below the top edge of the skirt. Consequently, almost any displacement of the guard may allow some particles to escape and 1.27 cm (0.5 in.) will offer no interference at all. This paper examines the development of an escape geometry characterized by Δ. Three methods of analysis are employed: rough analytical approximations, simple static testing of the guard, and dynamic wheel breakage testing.

The stochastic nature of friction will not allow anything better than a first order approximation of forces and energy dissipation. Grinding wheels may fracture at working speeds because of trauma introduced in the work environment. The statistical nature of grinding wheel materials may lead to overspeed disintegration at proof test speeds and greater. For the 22.9 cm (9 in.) diameter, 7.11 mm (0.280 in.) thick, 0.709 kg (1.5625 lb) type 27 grinding wheel studied in this paper, guard behavior will be investigated
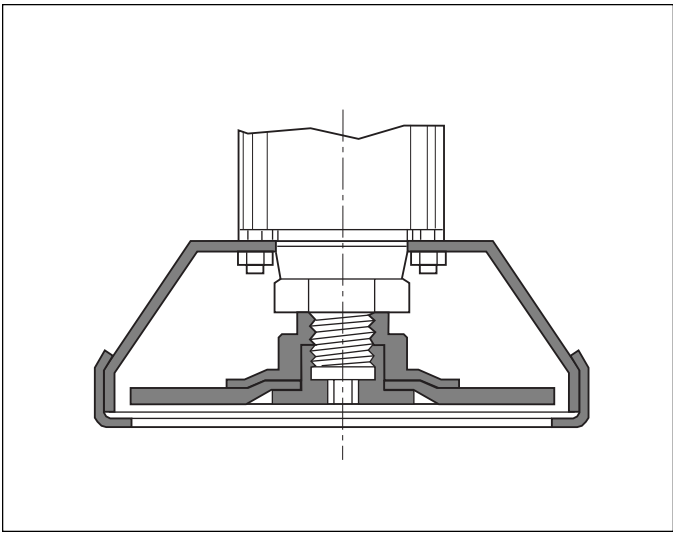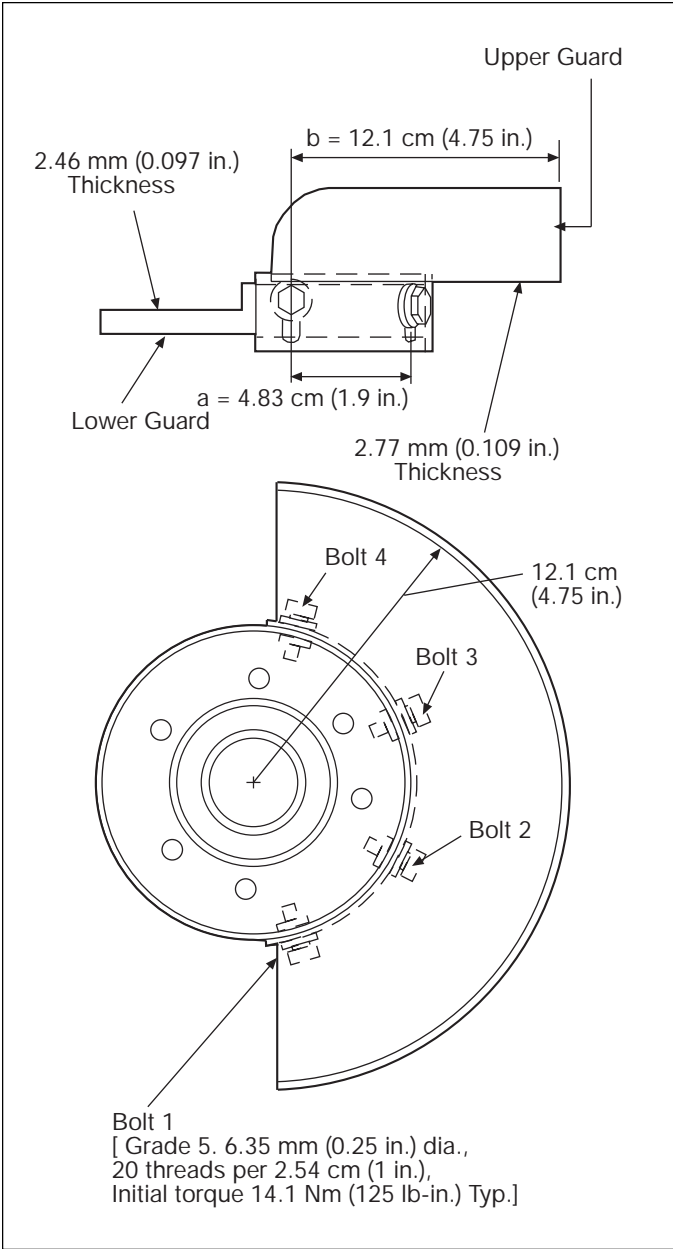

Figure 1. Typical type 27 wheel guard

Figure 2. Two piece adjustable guard in fully retracted position

2
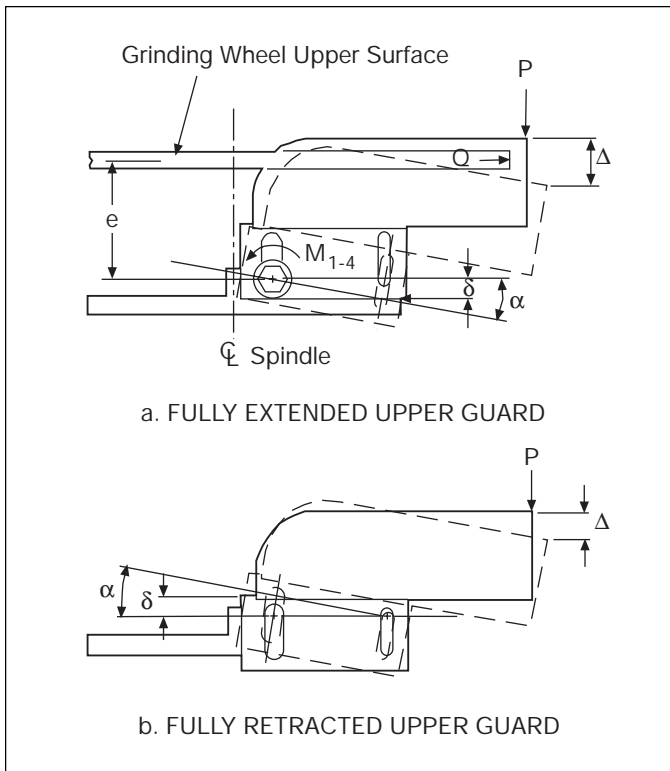
Figure 3. Rigid body rotation of upper guard

Figure 4. Load – deflection diagram for fully extended upper guard (Bolts 1 and 4 torqued to 14.1 Nm (125 lb-in.), bolts 2 and 3 absent)
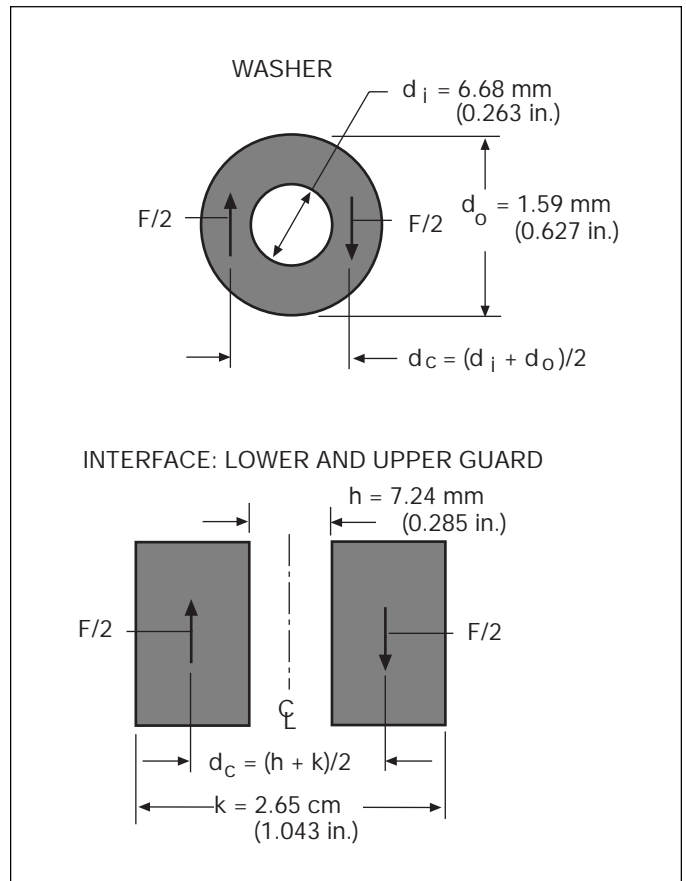
Figure 5. Friction surface footprints

for a rated working speed of 6,000 rpm, a proof test speed of 9,000 rpm, and a typical high speed fracture of 12,000 rpm. The rough calculations of resistance ignore elastic behavior and concentrate strictly on frictional resistance and frictional energy absorption at the location of bolts 1 through 4. The loading environment is approximated by examining available energy and by considering rate of change of momentum.

ROUGH ANALYTICAL APPROXIMATIONS

Preload Versus Torque
When a nut and bolt are tightened, the torque T gives rise to a clamping or preload force F_c. Shigley and Mischke (4) describe the following simple relationship between T and F_c which is independent of whether the threads are coarse or fine:

$$T \approx 0.20 F_c d \tag{1}$$

where d is the bolt diameter. Using a torque of 14.1 Nm (125 lb-in.) on a 6.35 mm (0.25 in.) diameter bolt, we obtain a clamping force F_c of 11,121 N (2,500 lb).

Coefficient of Friction
The determination of the frictional resistance and energy dissipation associated with the movement of the upper guard relative to the lower guard requires that we establish the coefficient of friction μ between the metal elements. Using the simple test setup shown in Fig. 3a where bolts 1 and 4 are torqued to 14.1 Nm (125 lb-in.) and bolts 2 and 3 are absent, a load-deflection diagram may be obtained as shown in Fig. 4. Here, a concentrated downward acting load P is applied to the leading edge of the upper guard using a universal testing machine. The measured response Δ is the deflection directly under the load.

Because of our choice of P and Δ, the area under the load-deflection diagram represents the work applied to the upper guard, U_{1-4}. For example, at Δ = 1.27 cm (0.5 in.), Fig. 4 shows U_{1-4} = 2.86 Nm (25.3 lb-in.). By taking moments about the line through bolts 1 and 4, the ordinate of the load-deflection diagram may be related to the frictional rotational resistance M_{1-4} by the formula:

$$M_{1-4} = bP \tag{2}$$

where b is the moment arm of P. Referring to Fig. 4, we observe a constant resistance P = 250 N (56.2 lb) which corresponds through equation 2 to 30.3 Nm (268 lb-in.).

3

To develop a formula for M_{1-4}, we first note that the upper guard skirt is sandwiched between a washer and the skirt of the lower guard. The footprints or contact areas associated with the washer and interface of the guard skirts is illustrated in Fig. 5. The frictional moment resistance M_w due to the washer is approximated in machine design textbooks (5) as:

$$M_w = \frac{\mu F_c d_c}{2} \tag{3}$$

where d_c is the mean washer diameter. We adopt the same formula for the rotational interface resistance M_I where d_c is taken as the distance between the pressure centers of the two rectangular contact areas as shown in Fig. 5. Accounting for bolts 1 and 4, $M_{1-4} = 2(M_w + M_I)$ or:

$$M_{1-4} = mF_c \left[\frac{d_i + d_o}{2} + \frac{h + k}{2} \right] \tag{4}$$

where d_i, d_o, h and k are defined in Fig. 5. Since M_{1-4} is equal to bP, we may determine $\mu = 0.0965$ from:

$$\mu = \frac{2bP}{F_c \left(d_i + d_o + h + k \right)} \tag{5}$$

Fully Extended Upper Guard

Resistance. Referring to Fig. 3a, we observe that rotation of the guard takes place about bolts 1 and 4. Resistance to this rotation is provided by the frictional rotational resistance of bolts 1 and 4, M_{1-4}, and by the sliding resistance F_s of bolts 2 and 3 which provide rotational resistance aF_s. The sliding resistance is created by the four surfaces which sandwich the upper guard skirt under a clamping force F_c, thus:

$$F_s = 4F_c \mu \tag{6}$$

The total resisting moment $M_{1-4} + aF_s$, can be used to resist the moment of an exploding grinding wheel force Q, i.e., eQ where e is shown in Fig. 3a as the height of the center plane of the grinding wheel above the bolt line 1-4. Furthermore, the total resisting moment may be used to resist the external moment Pb which arises from our static testing described later; thus:

$$Qe = Pb = M_{1-4} + aF_s \tag{7}$$

Using equations 4, 6 and 7, we obtain:

$$P = \frac{\mu F_c}{2b} \left(d_i + d_o + h + k + 8a \right) \tag{8}$$

and

$$Q = \frac{b}{e} P \tag{9}$$

Taking the worst case scenario for an exploding type 28 wheel located just even with the top edge of the guard, e= 6.03 cm (2.375 in.). Then, P=1,966 N (442 lb) and Q=3,932 N (884 lb).

Energy Absorption. A rigid body rotation α of the upper guard about the bolt line 1-4 gives rise to a displacement Δ of the leading edge of the guard. For small rotations, $\alpha \approx \Delta/b$ and the total energy dissipated at the friction joints, $U_{extended}$, is the product of α and the total resisting moment $M_{1-4} + aF_s$, or equivalently, $P\Delta$; thus:

$$U_{extended} = \frac{\Delta}{b} \left(M_{1-4} + aF_s \right) = P\Delta \tag{10}$$

For Δ= 1.27 cm (0.5 in.) and P = 1,966 N (442 lb), $U_{extended}$ is 25.0 Nm (221 lb-in.) and α=6.0°; for Δ=2.54 cm (1 in.), $U_{extended}$ is 49.9 Nm (442 lb-in.) and α=11.9°.

Fully Retracted Upper Guard

Resistance. When fully retracted to accommodate a type 27 grinding wheel, the upper guard may exercise a rigid body rotation about the bolt line 2-3 as shown in Fig. 3b. Ignoring any elastic or frictional resistance from bolts 2 and 3, a rotational resistance aF_s arises from the sliding action of bolts 1 and 4 in their slots. The normal rotational resistance M_{1-4} will not occur in this guard configuration because the relative velocities of translation will dominate the rotational velocities effectively eliminating frictional rotational resistance (6). Setting the two types of external moments about the bolt line 2-3, P(b-a) and Qe, equal to the resisting moment aF_s we obtain:

$$P(b-a) = Qe = a(4F_c \mu) \tag{11}$$

where F_c can be found by equation 1. Hence,

$$P = \frac{4aF_c \mu}{b-a} \tag{12}$$

$$Q = \frac{b-a}{e} P \tag{13}$$

When fully retracted, the subject type 27 grinding wheel gives an e=3.76 cm (1.48 in.). Therefore, P=2,860 N (643 lb) and Q=5,511 N (1,239 lb).

Energy Absorption. For small angles α, the displacements Δ and δ are related approximately as:

$$\frac{\delta}{a} = \frac{d}{b-a} = \alpha \tag{14}$$

The energy $U_{retracted}$ dissipated during a rigid body displacement Δ is given either by δF_s or ΔP. Thus:

$$U_{retracted} = \frac{4aF_c \mu \Delta}{b-a} \tag{15}$$

For Δ=1.27 cm (0.5 in.) and P=2,860 N (643 lb), $U_{retracted}$ is 36.3 Nm (321 lb-in.) and α=10°.

Load Environment

Energy. Overspeeding typically fractures a grinding wheel into three or four segments (7). At working speeds, trauma may lead to fractures that cannot be characterized. Consequently, one can imagine that the guard may be called upon to manage the kinetic energy of trapped segments from 1/4 to 2/3 of the original wheel mass. Because the guard and grinding wheel exhibit elastic behavior which absorbs very little energy, the friction joints must

Table 1 Kinetic energy of grinding wheel segments

Speed (rpm)	ω (rad/s)	Kinetic Energy – Nm (lb-ft)			
		Full Wheel	1/4 Wheel	1/2 Wheel	2/3 Wheel
Working: 6,000	628	912 (673)	228 (168)	457 (357)	609 (449)
Proof Test: 9,000	942	2,054 (1,515)	514 (379)	1,028 (758)	1,369 (1,010)
Typical Fracture: 12,000	1,257	3,653 (2,694)	914 (674)	1,826 (1,347)	2,435 (1,796)

Table 2. Guard reaction force Q_f – fluidized grinding wheel particles.

Speed (rpm)	Impinging Force, Q_f – N (lb)
Working: 6,000	10,173 (2,287)
Proof Test: 9,000	22,886 (5,145)
Typical Fracture: 12,000	40,688 (9,147)

dissipate any lost kinetic energy. For a rotating disk, the kinetic energy K.E. is given by Hibbeler (8) as:

$$K.E. = \frac{WR^2}{4g}\omega^2 \tag{16}$$

where W is the weight of a grinding wheel of radius R, g is gravitational acceleration and ω is the rotational speed in radians per second. Using equation 16, Table 1 is constructed for a 22.9 cm (9 in.) diameter grinding wheel weighing 0.709 kg (1.5625 lb) with a working speed of 6,000 rpm, a proof test speed of 9,000 rpm and a typical fracture speed of 12,000 rpm. Recall that our calculations, which overestimate the energy dissipation capacity, give the following estimates for a 1.27 cm (0.5 in.) displacement of the leading edge of the guard skirt: $U_{extended}$=25.0 Nm (221 lb-in.) and $U_{retracted}$=36.3 Nm (321 lb-in.). These dissipation levels are one to two orders of magnitude less than the available energies shown in Table 1.

Force. Consider the extreme case of a grinding wheel which disintegrates into a frictionless fluid which enters and leaves the guard at the same velocity as illustrated in Fig. 6. Here, the guard acts as a fixed vane with the same kinetic energy entering the guard as leaving it. The time rate of change of momentum of the grinding wheel particles rotating around the guard gives rise to a force Q_f which impinges on the guard skirt. The standard fluid mechanics formula for Q_f is (9):

$$Q_f = 2\left(\frac{\gamma}{g}\right)\Delta_o\, V^2 \approx \frac{WR\omega^2}{\pi g} \tag{17}$$

This equation is used to develop Table 2 where Q_f is tabulated for the same grinding wheel considered in Table 1. The forces in Table 2 can be compared to the frictional resisting forces computed for the extended and retracted upper grinding wheel guard, i.e., Q=3,932 N (884 lb) for the extended guard and Q=5,511 N (1,239 lb) for the retracted guard. Clearly, the assumed force environment will cause the upper guard to rotate to produce a leading edge displacement greater than 1.27 cm (0.5 in.).

Overspeeding a grinding wheel usually leads to the development of radial cracks. The two radial cracks shown in Fig. 7 have released a circular sector of 2β which is assumed to contact the
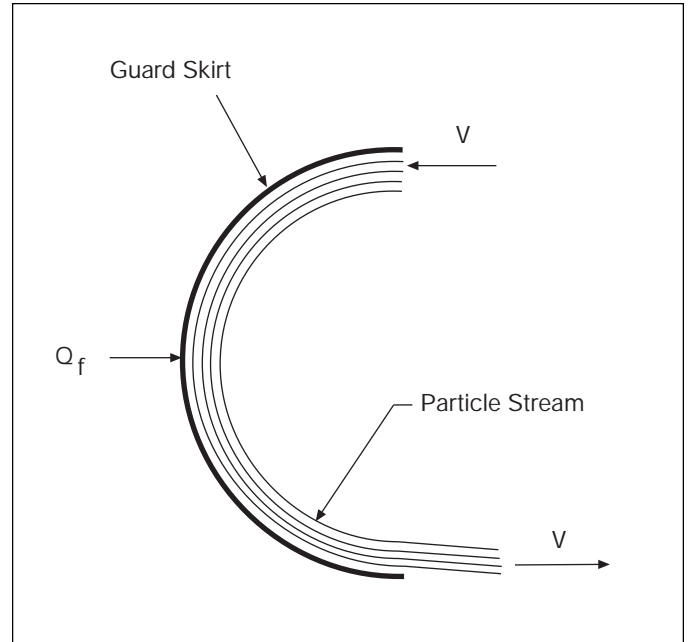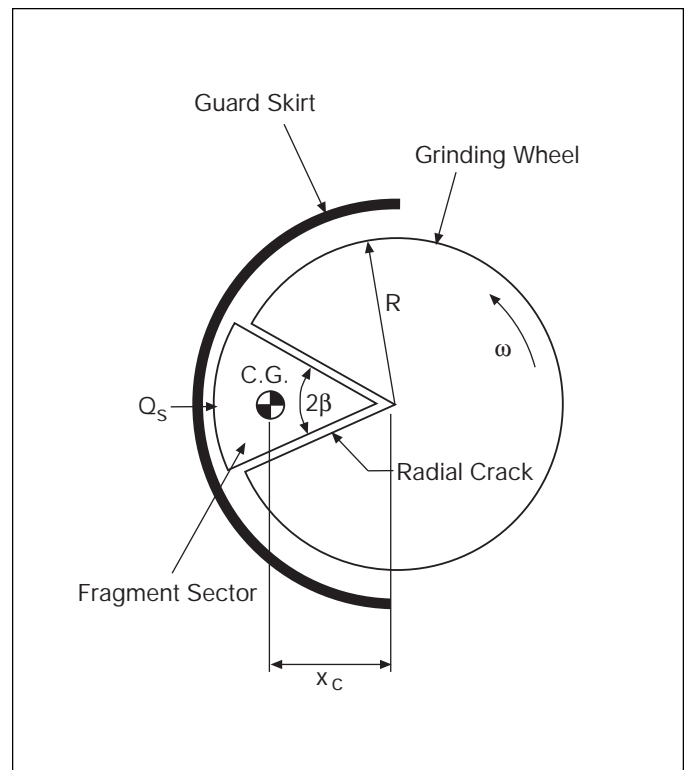

Figure 6. Grinding wheel guard as a fixed vane

Figure 7. Centrifugal force Q_s caused by rotating segment

5

guard skirt without friction and to be swept along at a rotational speed of ω. The center of gravity (C.G.) of the sector is located a distance x_c from its vertex which is also the spindle location. Equation 18 is a general formula for x_c:

$$x_c = \frac{2R\sin\beta}{3\beta} \qquad (18)$$

The centrifugal force Q_s developed by the grinding wheel sector reacts against the guard skirt with a magnitude given by the standard formula (10):

$$Q_s = mx_c\omega^2 = \left(\frac{WR\omega^2}{\pi g}\right)\frac{2}{3}\sin\beta = \left(Q_f\frac{2}{3}\sin\beta\right) \qquad (19)$$

where m is the sector mass and x_c is taken from equation 18. Since $2/3\sin\beta$ is always less than unity, it would appear that the segment forces Q_s are less than the fluidized grinding wheel forces Q_f for the same speed of rotation ω. The sector forces Q_s that impinge on the guard skirt have been tabulated in Table 3 for the subject grinding wheel for various speeds, sector sizes and combinations. All of the forces in Table 3 will cause the upper guard to tilt forward creating a displacement Δ of the leading edge of the guard.

STATIC TESTING

Test Setup
In the fully retracted or the fully extended positions, rigid behavior of the upper guard produces a rotation about bolt lines 2-3 or 1-4 respectively. It is this pure rotation that dissipates energy through friction and consequently any method of applying a tilting couple to the guard is acceptable for studying energy absorption. Since it was convenient to mount the guard in a universal testing machine with its spindle axis vertical and since a vertical concentrated load could be applied at the very portion of the skirt where we characterize the maximum escape displacement, we have chosen the test setup illustrated in Fig. 3 where Q is ignored. Recall that the area under a load-deflection
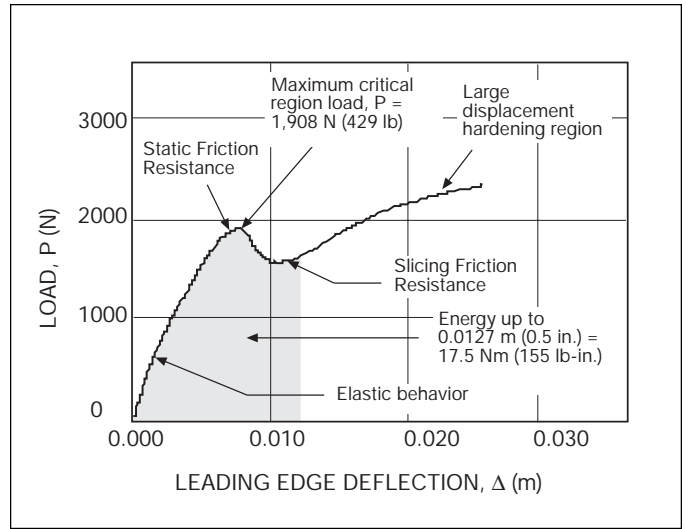

Figure 8. Load–deflection diagram for fully extended upper guard [Bolts 1 through 4 torqued to 14.1 Nm (125 lb-in.)]
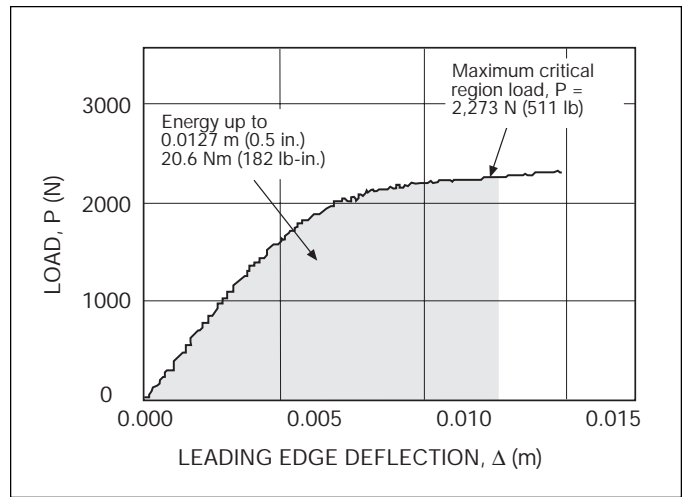
Figure 9. Load–deflection diagram for fully retracted upper guard [Bolts 1 through 4 torqued to 14.1 Nm (125 lb-in.)]

Table 3. Guard reaction force Q_s – sectors of grinding wheel
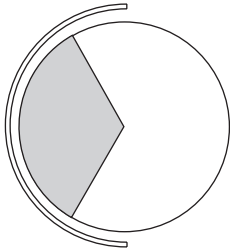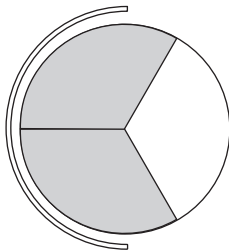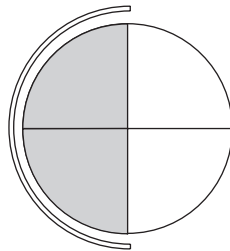
Impinging Force, Q_s – N (lb)			
Speed (rpm)	120° Segment	One 240° Segment or Two 120° Segments	One 180° Segment or Two 90° Segments
Working: 6,000 Proof Test: 9,000 Typical Fracture: 12,000	5,872 (1,320) 13,211 (2,970) 23,491 (5,281)	5,872 (1,320) 13,211 (2,970) 23,491 (5,281)	6,784 (1,525) 15,257 (3,430) 27,125 (6,098)

diagram PΔ represents the work performed on the guard to bring it to any displacement Δ of interest.

Fully Extended Guard Test Results

For the fully extended guard, a load-deflection diagram is shown in Fig. 8 which illustrates the guard behavior through a displacement equal to 2.54 cm (1 in.). In the critical displacement from zero to 1.27 cm (0.5 in.), the maximum recorded load was 1,908 N (429 lb) which can be compared to the predicted load of 1,966 N (442 lb). In the same region, the absorbed energy is 17.5 Nm (155 lb-in.) which is lower than the calculated $U_{extended}$ equal to 25.0 Nm (221 lb-in.). The total area under the curve up to Δ equal to 2.54 cm (1 in.) corresponds to 59.9 Nm (535 lb-in.) whereas the rough calculations indicated 49.9 Nm (442 lb-in.).

The testing program as characterized by the load-deflection diagram in Fig. 8 provides a richer understanding of the upper guard behavior. Elastic behavior analysis can be observed for displacements up to 7.62 mm (0.3 in.). It is here that the maximum resistance is achieved which corresponds to static friction. When Δ is between 7.62 mm (0.3 in.) and 1.02 cm (0.4 in.), the resistance falls off as the sliding friction is activated at the joints. For displacements greater the 1.02 cm (0.4 in.), the resistance hardens because of large displacement effects including binding of the bolts.

The assumption of rigid-friction behavior used in our analysis overestimates the absorption capability which involves elastic behavior. During a fragment storm, our static test results would indicate that the escape displacement has a very large elastic component. Indeed, when a wheel is mounted close to the top of the guard skirt, the elastic displacements alone will produce an escape geometry for the broken wheel fragments. The rigidity of even single piece guards must be carefully evaluated to be certain that their rigidity is sufficient to achieve the protection required by ANSI.

Fully Retracted Guard Test Results

The load-deflection diagram shown in Fig. 9 describes the behavior of the upper guard in its fully retracted position. In the critical displacement region Δ equal to 1.27 cm (0.5 in.), the maximum load was measured as 2,273 N (511 lb) which can be compared to our analytical prediction of 2,860 N (643 lb). Further, the energy absorbed up to the maximum displacement Δ equal to 1.27 cm (0.5 in.) was found to be 20.6 Nm (182 lb-in.) which can be compared to our prediction of 36.3 Nm (321 lb-in.). In the critical region up to Δ equal to 1.27 cm (0.5 in.), elastic behavior
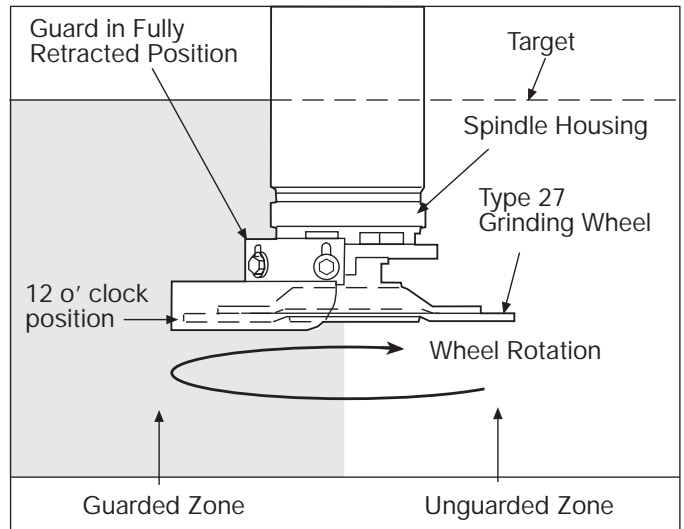

Figure 10. Dynamic test setup

dominates the first 50% of the curve. Once again, elastic behavior alone produces an escape geometry for wheels mounted close to the top of the guard skirt. It should be noted that the bolts utilized in our static testing program were preloaded to a torque of 14.1 Nm (125 lb-in.) which corresponds to the "as manufactured" condition associated with the guard. The stochastic nature of friction leads to very large variations in the preload determinations F_c. Shigley and Mischke show a range of values from 23.6 kN (5,305 lb) to 42.7 kN (9,599 lb) when the bolt torque value is held constant at 90 Nm (797 lb-in.) (4). In view of the large scatter associated with frictional behavior, it is difficult to justify a refined analytical investigation of guard behavior.

DYNAMIC WHEEL BREAKAGE TESTING

Test Setup

Referring to the dynamic test setup shown in Fig. 10, the test wheel was mounted onto a variable speed spindle. The spindle housing was used to mount the two piece adjustable depressed center wheel guard described in Fig. 2 in a downward attitude. The test was conducted with the upper guard in the fully retracted position which placed the outer surface of the wheel 6.35 mm (0.25 in.) from the top edge of the upper guard skirt. Using this configuration, the spindle speed was gradually increased until the grinding wheel fragmented into four major pieces at 11,500 rpm. The fragments impinged on a cylindrical target located concentrically with the spindle axis. Fig. 11 maps the imprint of the fragments on the target where the guarded and unguarded zones are differentiated.
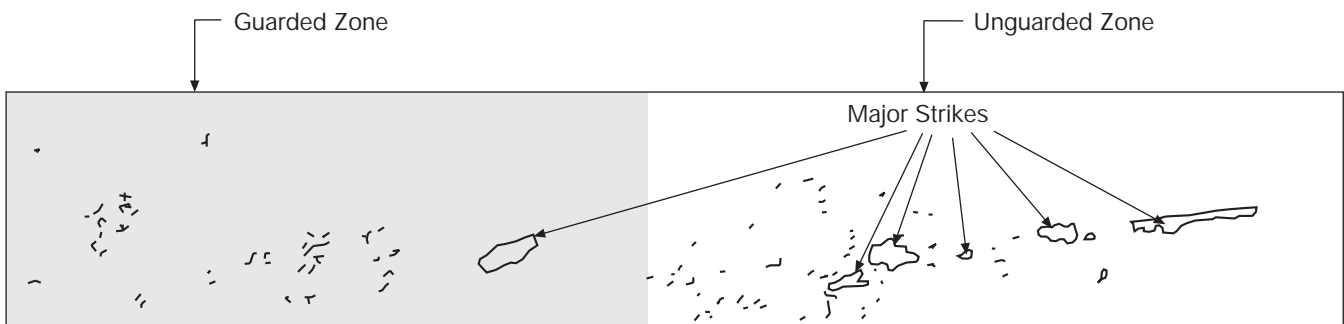

Figure 11. Dynamic test target

Test Results

Following the dynamic testing, the following observations were noted:

1. Major and minor strikes appear on the target in the guarded zone.
2. Major and minor strikes appear on the target in the unguarded zone.
3. Major strikes are collinear on the target outside the wheel's plane of rotation.
4. Minor strikes on the target exhibit a spray pattern.
5. No plastic deformation of the upper guard with the exception of small zones in the leading and trailing edges of the upper skirt.
6. Rigid body rotation α of the upper guard was 10.5 degrees. All bolt sliding occurred at bolts 1 and 4.
7. Upper guard leading edge deflection Δ took a permanent set of 1.59 cm (0.625 in.).
8. Scratches appear on the inside of the upper guard in the rotational plane of the wheel as depicted in Fig. 12.
9. Secondary breakage of the wheel produced witness marks toward the mounting side of the guard skirt.
10. Witness marks on the right side of the guard indicate fragment trajectories into the guarded zone.
11. Witness marks indicate helical trajectories into the guarded zone.
12. After remounting the dynamic test guard and a new wheel on its grinder, there is line of sight to the wheel's plane of rotation from the 12 o'clock position, i.e., an escape geometry was established.

CONCLUSIONS

The purpose of the guard is to act as a sentinel against worst case wheel fragmentation scenarios. The rough calculations which overestimate the resistance of the guard indicate that the guard design is hopelessly inadequate. Static testing indicates that the guard resistance is even lower than predicted and that elastic deflections alone create an escape geometry in addition to the rigid body displacements. Based on either the rough calculations or the static testing, it is no surprise that the dynamic test decisively establishes the inadequacy of this two piece depressed center wheel guard. In spite of the fact that the tilting guard will shed fragments with their associated kinetic energy, the available forces and energies are so high that the guard achieved its maximum tilt angle which was restricted by large displacement binding of the bolts.

If multiple dynamic tests are performed, each will produce failures at different speeds and different fragmentation modes due to primary and secondary fractures. It should be noted that the clearance between the periphery of a new wheel and the inside of the guard skirt is only 6.35 mm (0.25 in.). Any fragments wedged or jammed in this space that inhibit wheel particles from exiting the guard will produce impacts with their associated forces and impulses that will act on the skirt. Because of the high energies available in grinding wheels at both working and fracturing speeds, very large reaction forces may be experienced by the skirt.

The results of our analysis, static testing, and dynamic testing all suggest that dynamic testing evaluation is essential for all
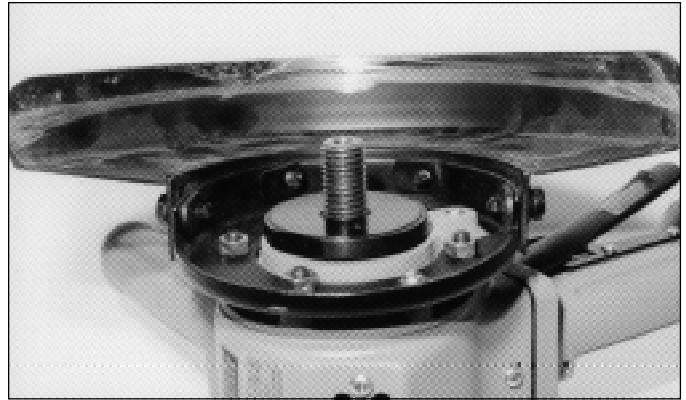

Figure 12. Scratches on upper guard after dynamic wheel breakage testing

adjustable two piece guards including depressed center and cup wheel guards. Both classes of adjustable two piece guards provide a rigid body escape geometry in addition to the displacements caused by deflection, yielding, and fracturing that may take place in a guarding system. Finally, our results indicate that targets must be used to establish the performance capability of guards which may fail elastically by permitting escape deflections. Without the target, one can draw false conclusions based on the lack of permanent displacements or distortions of the guard structure. For example, a rubber guard would appear unscathed during a grinding wheel excursion even though fragments were fully penetrating the guarded zone.

REFERENCES

1. "American National Standard Safety Code for Portable Air Tools," *ANSI B186.1-1975*, American National Standards Institute, New York, Nov. 20, 1975.
2. "American National Standard Safety Code for Portable Air Tools," *ANSI B186.1-1975*, American National Standards Institute, New York, Nov. 20, 1975, p. 14.
3. "American National Standard Safety Code for Portable Air Tools," *ANSI B186.1-1975*, American National Standards Institute, New York, Nov. 20, 1975, p. 21.
4. Shigley, J.E. and Mischke, C.R., *Mechanical Engineering Design*, 5th ed., McGraw-Hill, New York, 1989, p. 346.
5. Shigley, J.E. and Mischke, C.R., *Mechanical Engineering Design*, 5th ed., McGraw-Hill, New York, 1989, p. 332.
6. Timoshenko, S. and Young, D.H., *Vibration Problems in Engineering*, 3rd ed., D. Van Nostrand, New York, 1955, p. 68.
7. Suzuki, I. and Wada, R., Schleifscheibenbruch wahrend der Rotation," *Werkstatt und Betrieb*, Vol. 105, No. 9, Sept. 1972, pp. 643-647.
8. Hibbeler, R.C., *Engineering Mechanics - Dynamics*, 6th ed., MacMillan, New York, 1992, p. 378.
9. Streeter, V.L., *Fluid Mechanics*, 1st ed., McGraw-Hill, New York, 1951, p. 101.
10. Timoshenko, S. and Young, D.H., *Engineering Mechanics*, 3rd ed., McGraw-Hill, New York, 1951, p. 407.

SAFETY BRIEF